J Mol Model (2013) 19:2299–2308
DOI 10.1007/s00894-013-1774-3

ORIGINAL PAPER

Excited-state relaxation paths of oxo/hydroxy and N9H/N7H tautomers of guanine: a CC2 theoretical study

Vassil B. Delchev

Received: 27 October 2012 / Accepted: 15 January 2013 / Published online: 6 February 2013

Abstract We performed a theoretical investigation, at the CC2/aug-cc-pVDZ level, of the ring-deformation mechanisms of four guanine tautomers (oxo, hydroxy, N9H, and N7H). The study showed that the optimized conical intersections S_0/S_1 are accessible through the $^1\pi\pi^*$ excited states of tautomers. The optimized conical intersections S_0/S_1, which show deformation at the pyrimidine ring, have high energies. This means that the relaxations of the $^1\pi\pi^*$ excited states via internal conversion are disfavored. For two tautomers we found crossing points $^1\pi\pi^*/^1\pi\sigma^*$ of the excited-state reaction paths, revealing the possibility of a population of the $^1\pi\sigma^*$ excited state by the $^1\pi\pi^*$ excited state.

Keywords CC2 calculation · Conical intersection · Excitation energy · Excited state · Guanine

Introduction

Guanine is a major building block in nucleic acid macromolecules. Among the five nucleobases present in DNA and RNA, cytosine and guanine show tautomerism and tautomeric forms in the gas phase, whereas uracil, thymine, and adenine exist only as single tautomers [1–6]. The most significant tautomeric conversion is the oxo-hydroxy conversion [1]. N9H and N7H tautomers of oxo and hydroxy guanine have been observed by Nir and Choi [2, 7].

The thermodynamic stability of tautomers of guanine has been the subject of many theoretical papers [2, 8, 9]. A theoretical investigation by Plekan et al. [1] at the MP2, CCSD, and CCSD(T) theoretical levels, revealed that the N7H oxo guanine tautomer is the most stable form in the ground state. The stability of this tautomer in the gas phase is kept even at 600 K [1].

Nucleic acid bases are major chromophores in nucleic acid macromolecules. The photostability of pyrimidine nucleobases has been explained by the ultrafast deactivation of excited states through deformation of aromatic rings at C=C bonds, i.e., twisting [10–14]. The driven state is the $^1\pi\pi^*$ excited state, which leads to conical intersections S_0/S_1 [13, 14]. Recently, Yamazaki et al. [15] reported barrierless deactivation paths of the $^1\pi\pi^*$ excited state of the biologically relevant N9H oxo guanine tautomer. They found a conical intersection S_0/S_1 mediating this process. The geometry of the conical intersection is highly deformed at the amino group of the compound [15]. Unfortunately, the mechanisms of ring deformations of the remaining tautomers (oxo, hydroxy, N9H, and N7H) are still unknown. Nevertheless, we suppose that the driven state in these tautomers is $^1\pi\pi^*$.

The purpose of the current research was to investigate the deactivation mechanisms of the guanine tautomers connected with deformation of the purine ring. Clarification of this problem requires optimization of the conical intersections S_0/S_1 mediating excited-state relaxation processes.

Computational methods

The ground-state equilibrium geometries of all planar tautomers of guanine were optimized at the coupled-cluster CC2 level using aug-cc-pVDZ basis functions (for calculation of vertical excitation energies) and at the CASSCF (6,6)/6-31G* level [for the linear interpolation in internal coordinates (LIIC) approach—excited-state reaction paths]. The equilibrium geometries of the $^1\pi\pi^*$ excited states of the tautomers were also found at the CC2 level. The emission

V. B. Delchev (✉)
Department of Physical Chemistry, University of Plovdiv,
Tzar Assen 24 Str.,
4000 Plovdiv, Bulgaria
e-mail: vdelchev@uni-plovdiv.net

energy is defined as the energy gap between the $^1\pi\pi^*$ state equilibrium geometry and the ground state at the $^1\pi\pi^*$ optimized structure.

The structures of the conical intersections and their gradient difference (GD) and derivative coupling (DC) vectors were found at the CASSCF(6,6)/6-31G* level. These vectors of each conical intersection were used to generate 49 geometries (points) on the narrow grid by displacement from the conical intersection geometry. The generated structures and their S_0 and S_1 energies were used to construct adiabatic surfaces (W_1 and W_2) around the conical intersections. The S_0 and S_1 energies for the construction of the adiabatic surfaces were calculated at the CASSCF(6,6)/6-31G* level to be consistent with the level of optimizations of the conical intersections. All CASSCF calculations were performed with two state-averaging states (S_1 and $^1\pi\pi^*$).

For the generation of structures on the narrow grid around the conical intersections, we orthogonalized the vectors g=2GD and h=DC using Yarkony's procedure [16]. The structures on the narrow grid were generated using displacements of 0.3 eV. The quasi-diabatization of the ab initio energies were performed by the procedure described in the paper of Woywod [17]. The quasi-diabatic wavefunction $\widetilde{\Psi}$ is obtained by the equation $\widetilde{\Psi} = S^T\Psi$ (Ψ- adiabatic wavefunction). In fact, the quasi-diabatic potentials V_{11}, V_{22}, and V_{12} are calculated by the equation

$$\begin{pmatrix} V_{11} & V_{12} \\ V_{12} & V_{22} \end{pmatrix} = S^T \begin{pmatrix} W_1 & 0 \\ 0 & W_2 \end{pmatrix}, \text{ where} \quad (1)$$

$$S = \begin{pmatrix} \cos\theta & -\sin\theta \\ \sin\theta & \cos\theta \end{pmatrix}$$

and

$$\theta = \frac{1}{2} tg^{-1} \frac{2H_{12}}{H_{11} - H_{22}}. \quad (2)$$

H_{11}, H_{12}, H_{22}—Hamilton matrix elements in the quasi-diabatic representation. They are expressed by the GD and DC vectors.

To maintain the limited active space (6/6) for the computations is critical to obtaining the optimized structures of conical intersections. Our experience shows that larger active spaces for conical intersection optimizations enhance the flexibility of the wavefunction and the changeability of the active space. Such optimizations lead to failures of the optimizations. The active orbitals of the N7H-oxo tautomer of guanine and its conical intersection S_0/S_1 with the deformed purine ring are depicted in Fig. 1.

All active orbitals are π/π^*-MO. We did not include other orbitals, e.g., n- or σ-MO, since it is known [10, 13, 14] that deformations of the aromatic rings lead to lowering of the energies of the $\pi\pi^*$ excited states. At the CASSCF level we are interested only in these states, especially near the conical intersections.

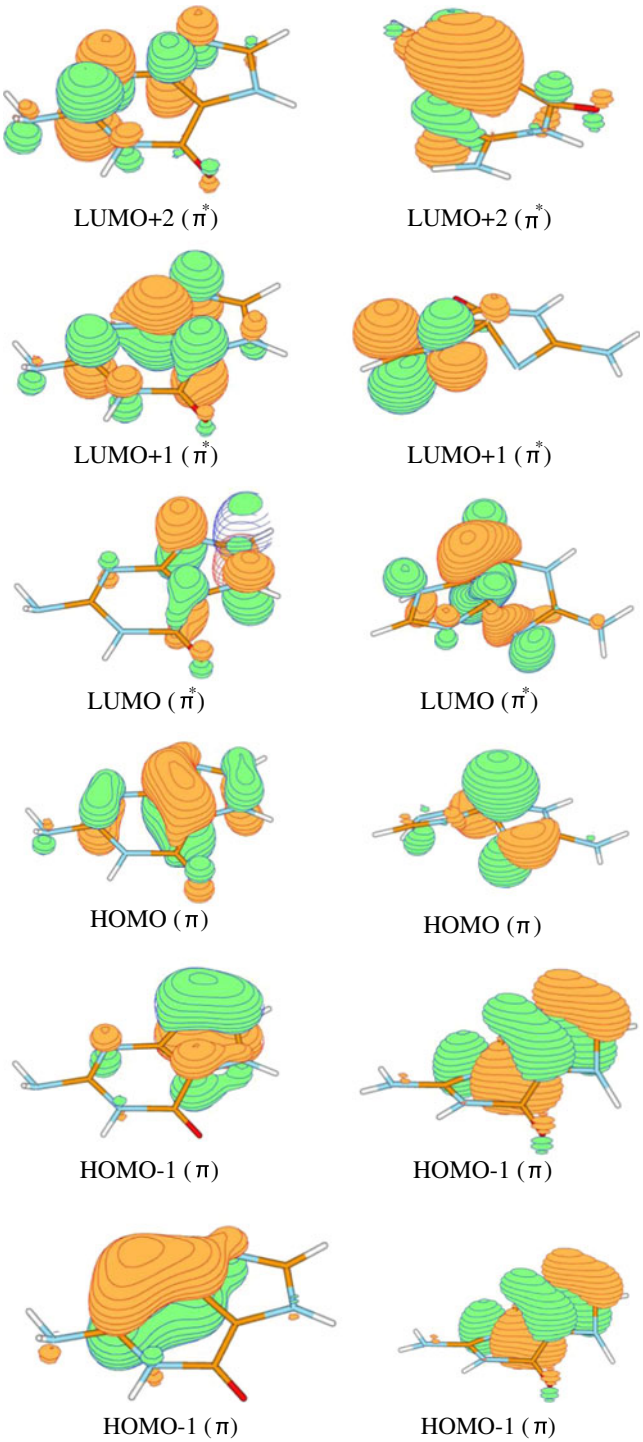

Fig. 1 Active orbitals of the ground-state equilibrium geometry of N7H-oxo tautomer of guanine and its conical intersection S_0/S_1 with the deformed purine ring

The LIIC approach was used to interpolate between a given ground-state minimum geometry and a certain conical intersection using the CC2//CASSCF protocol and aug-cc-pVDZ basis set: CC2 single-point computations with the CASSCF structures along the reaction coordinate. Each

internal coordinate Q_i of a given intermediate structure was found by the equation:

$$Q_i = Q_i(c) + \varepsilon.[Q_i(ci) - Q_i(c)], \quad (3)$$

where $Q_i(c)$ is the i-th coordinate of the initial structure (ground-state equilibrium geometry), whereas $Q_i(ci)$ is the same coordinate of the S_0/S_1 conical intersection; ε is an interpolation parameter. The interpolation parameter is either 0 (at the ground-state minimum geometry) or 1 (at the conical intersection). Second-order approximate coupled cluster singles and doubles (CC2) computations (aug-cc-pVDZ basis functions) were performed with the TURBOMOLE program system [18, 19]. CASSCF calculations were carried out with the GAUSSIAN 03 program package [20].

Results and discussion

Equilibrium geometries of the S_0 and $^1\pi\pi^*$ states

The current study focused on the oxo, hydroxy, and N9H/N7H tautomers of guanine. The CC2-optimized equilibrium geometries of the S_0 and $^1\pi\pi^*$ electronic states of guanine tautomers are presented in Fig. 2.

As can be seen, the ground-state equilibrium geometries are planar. Only the hydrogen atoms of the amino group deviate from the molecular plane. The $^1\pi\pi^*$ excited-state equilibrium geometry of tautomer A is also planar. Moreover, the hydrogen atoms of the amino group lie in the molecular plane. It was found that the bond lengths of the pyrimidine ring are elongated as compared to the ground-state structure. One exception is the N_1–C_2 bond, which is shorter in the excited state. The N–C bonds of the imidazole ring are longer in the excited state than in the ground state. Identical geometry changes in the excited state show also tautomer D.

As compared to the ground state, the $^1\pi\pi^*$ excited-state equilibrium geometry of tautomer B is highly deformed at the pyrimidine residue of the molecule. The N–C bonds in the pyrimidine ring are longer in the excited state than in the ground state. Both states show almost the same length of C_2–NH_2 bond. This excited-state equilibrium geometry is obtained despite the planar structure that was the starting point of the optimization. As can be seen, the $^1\pi\pi^*$ excited-state equilibrium geometry of tautomer C is also the same.

Vertical excitation energies and emission energies

The calculated vertical excitation energies of tautomers of guanine, found at the CC2/aug-cc-pVDZ level, are listed in Table 1.

The data show that the low-lying excited state of all tautomers is the spectrosopically active $^1\pi\pi^*$ excited state. For tautomers A, B and D, the $^1n\pi^*$ excited state has higher energy than the $^1\pi\sigma^*$ excited state. Furthermore, among the five lowest excited states of tautomer C, the $^1n\pi^*$ excited state is missing. The $^1\pi\pi^*$ emission energy of tautomer A is 3.808 eV, which is a reduction of 0.627 eV as compared to the vertical excitation energy. The emission energy of tautomer B is very low (0.206 eV) ,which shows that the $^1\pi\pi^*$

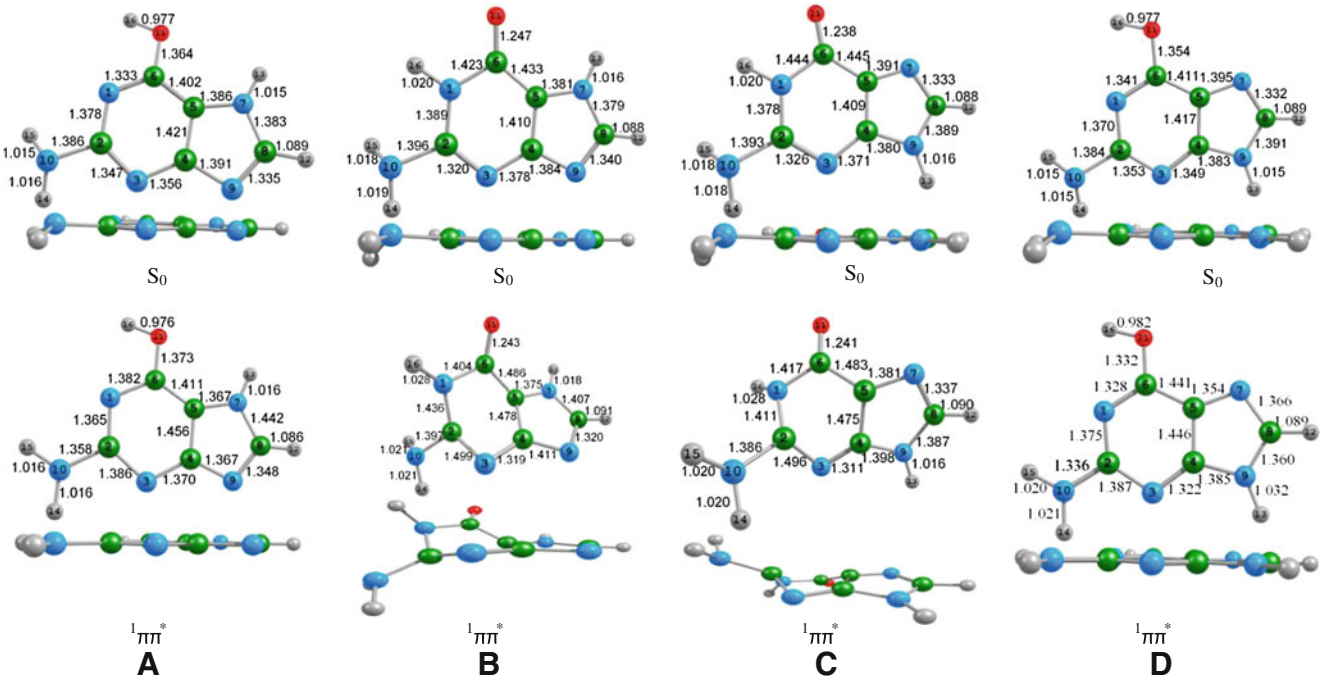

Fig. 2 CC2-equilibrium geometries of the electronic states S_0 and $^1\pi\pi^*$ of guanine tautomers

Table 1 Vertical excitation energies of guanine tautomers A–D

A		B		C		D	
State	eV	State	eV	State	eV	State	eV
$^1\pi\pi^*$	4.435	$^1\pi\pi^*$	4.755	$^1\pi\pi^*$	4.882	$^1\pi\pi^*$	4.746
$^1\pi\sigma^*$	5.042	$^1\pi\sigma^*$	5.064	$^1\pi\sigma^*$	4.958	$^1\pi\sigma^*$	5.113
$^1n\pi^*$	5.059	$^1n\pi^*$	5.159	$^1\pi\sigma^*$	5.294	$^1\pi\sigma^*$	5.391
$^1\pi\sigma^*$	5.350	$^1\pi\sigma^*$	5.359	$^1\pi\sigma^*$	5.306	$^1n\pi^*$	5.395
$^1\pi\pi^*$	5.593	$^1\pi\pi^*$	5.460	$^1\pi\pi^*$	5.368	$^1\pi\sigma^*$	5.486

excited-state equilibrium geometry of tautomer B is situated near a conical intersection S_0/S_1. The $^1\pi\pi^*$ emission energy of tautomer C is 0.720 eV., indicating that the minimum of the tautomer is also situated near a conical intersection S_0/S_1. Obviously, tautomers B and C should show a large Stocks shift in the fluorescent spectrum.

Conical intersections

For each tautomer we optimized three conical intersections at the CASSCF(6,6)/6-31G* level. For tautomer A we found only two conical intersections connected with deformation of the aromatic ring. As an initial structure, we used the deformed guanine tautomers, which resemble the well known conical intersections S_0/S_1 of pyrimidine nucleobases [10, 11]. Our intuition orientated us to look for conical intersections showing deformation of the imidazole ring. All geometries of the optimized conical intersections are depicted in Fig. 3.

As clear from the Introduction, a typical conical intersection S_0/S_1 of cytosine shows deformation of the pyrimidine ring at the NH_2 group [10]. Despite our best attempts, we were unable to find such a conical intersection of tautomer A of guanine.

The conical intersections S_0/S_1 connected with a deformation of the imidazole ring are designated with a subscript '1', whereas those showing deformation of the pyrimidine ring have the subscript '2'.

In order to prove that the conical intersections S_0/S_1 are real intersection points between the potential energy surfaces (PESs) of the S_0 and S_1 states, we investigated the adiabatic PESs W_1 and W_2 in a restricted area around each conical intersection. For a limited number of conical intersections, the potentials W_1 and W_2 were found, because of the flexibility of the wavefunction and the inconsistency of the active space 6/6. In these cases, where this approach failed, we calculated the adiabatic potentials W_1^* and W_2^* using the normal modes of the ground state equilibrium geometries. The corresponding quasi-diabatic potentials are designated by V_{11}^* and V_{22}^*. All PESs are presented in Fig. 4.

The constructed PESs showed that the conical intersections are the real mediators between the S_0 and S_1 excited states. Moreover, the adiabatic surfaces allow the reaction path on the PES of S_0 state after the internal conversion through the conical intersection to be traced. The adiabatic

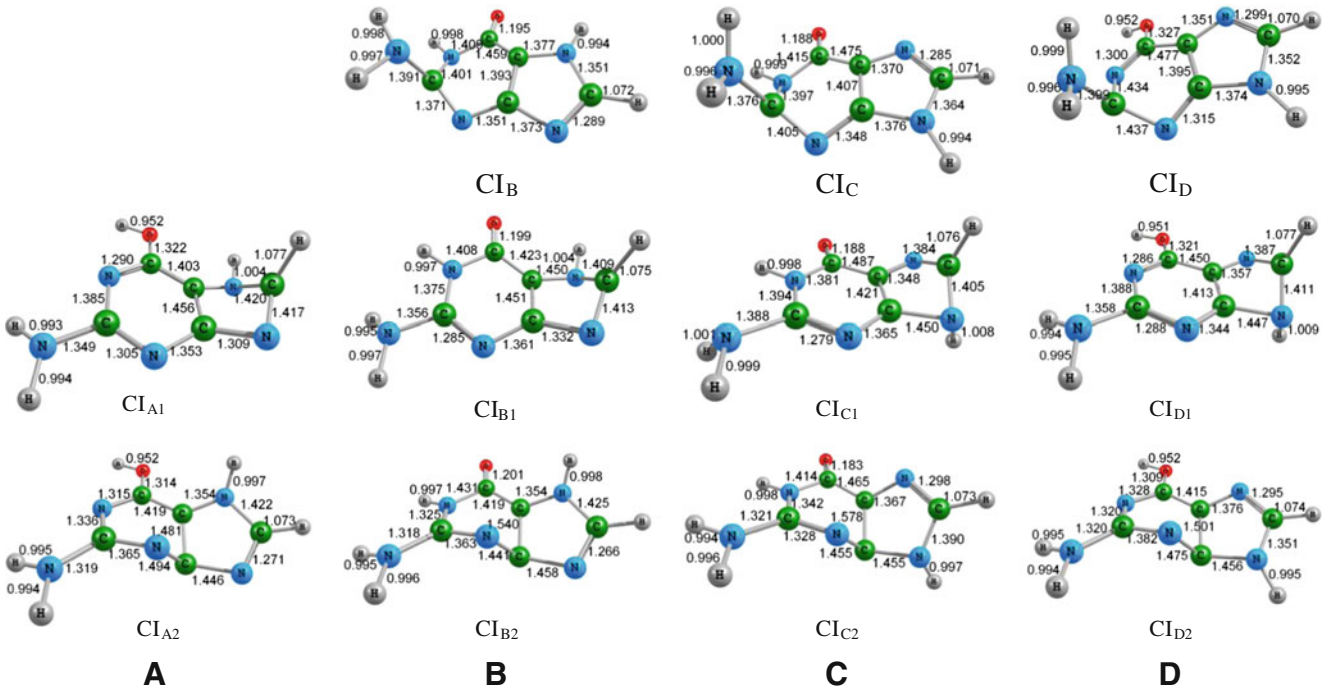

Fig. 3 Conical intersections S_0/S_1 of tautomers of guanine found at the CASSCF(6,6)/6-31G* level

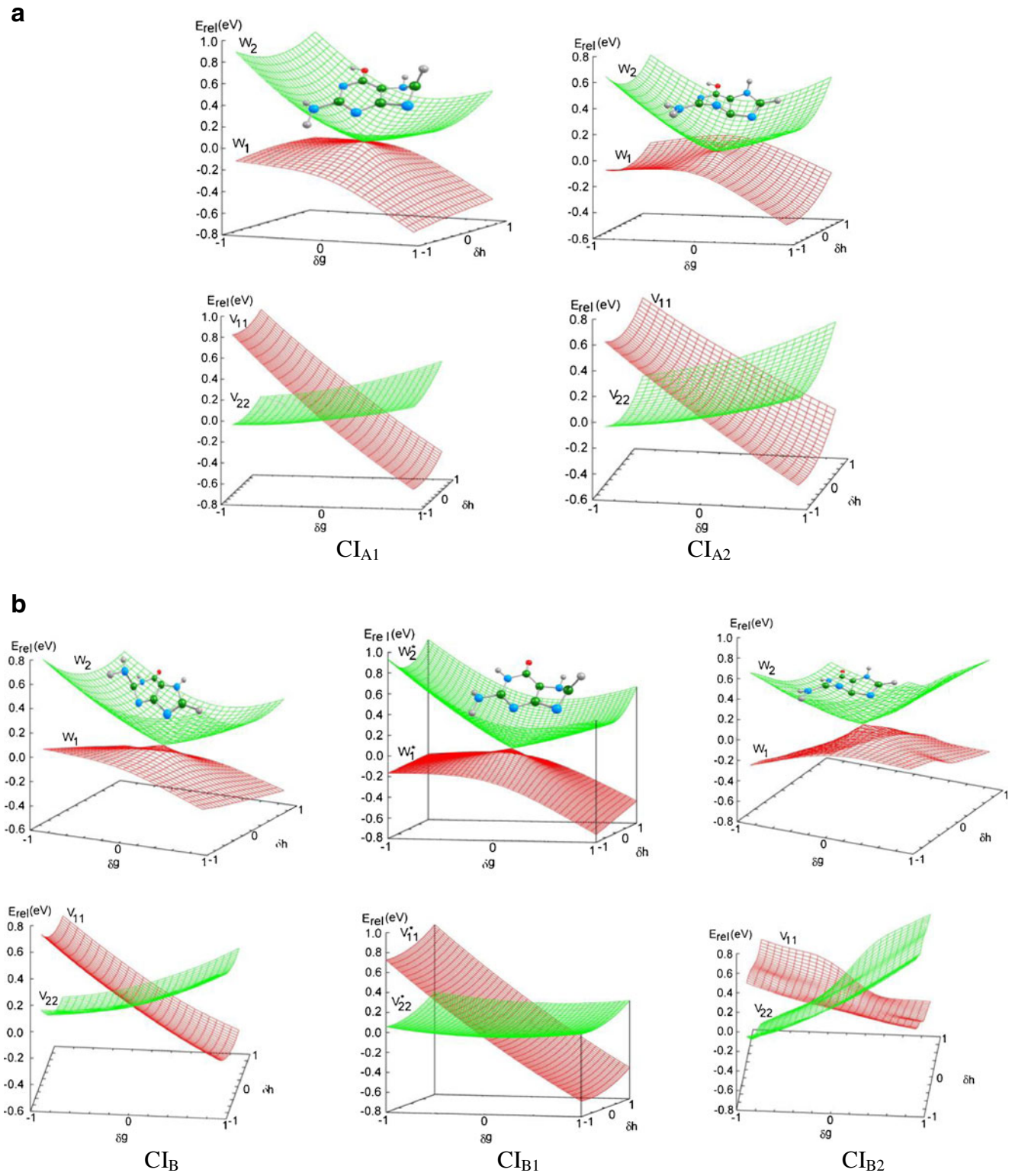

Fig. 4 CASSCF adiabatic and quasi-diabatic potential energy surfaces (PESs) round the conical intersections of tautomer (**a**) A, (**b**) B, (**c**) C, and (**d**) D of guanine

and quasi-diabatic surfaces of the conical intersection CI_{D2} are rather folded and wavy. There are two explanations for this finding: (1) flexible wavefunction and changeable active space near the conical intersection CI_{D2}; (2) closely situated minima and maxima of the electronic states in the studied area of the branching space.

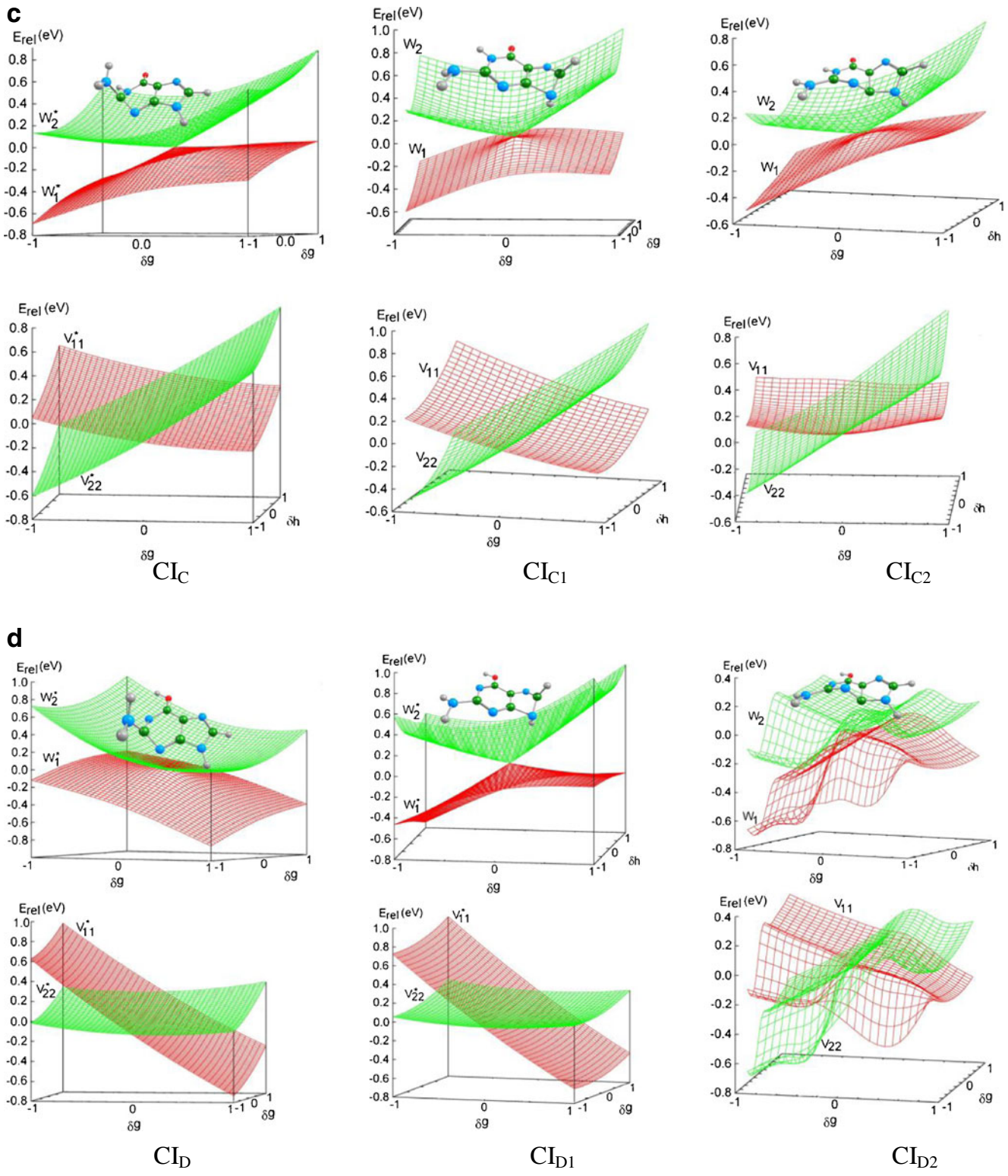

Fig. 4 (continued)

Excited-state reaction paths

In order to understand whether the conical intersections are accessible through some excited state we performed LIIC between the ground-state equilibrium geometries of the tautomers and the conical intersections S_0/S_1, both optimized at the CASSCF(6,6) level. The adiabatic energies of the electronic states along the reaction

coordinate were calculated by the CC2//CASSCF/aug-cc-pVDZ protocol.

The excited state reaction paths of tautomer A are illustrated in Fig. 5a. The $^1\pi\pi^*$ excited-state reaction path leads to the conical intersection CI_{A1} passing by a low energy barrier of 0.77 eV (74 kJ.mol^{-1}). With regard to the approach used, the $^1\pi\sigma^*$ and $^1n_N\pi^*$ excited-state reaction paths show an increase in energy. They have higher energies than the $^1\pi\pi^*$ excited-state reaction path. Figure 5b shows that the conical intersection CI_{A2} is accessible by the $^1\pi\pi^*$ excited-state reaction path. This mechanism implies a radiationless relaxation of the spectroscopically active $^1\pi\pi^*$ excited state vie internal conversion through the conical intersection CI_{A2}. The latter has higher energy than the energy of the conical intersection CI_{A1}. Moreover, the $^1\pi\pi^*$ excited-state reaction path shows two shallow minima separated by a low maximum. Both mechanisms in Fig. 5 indicate that tautomer A of guanine is photostable.

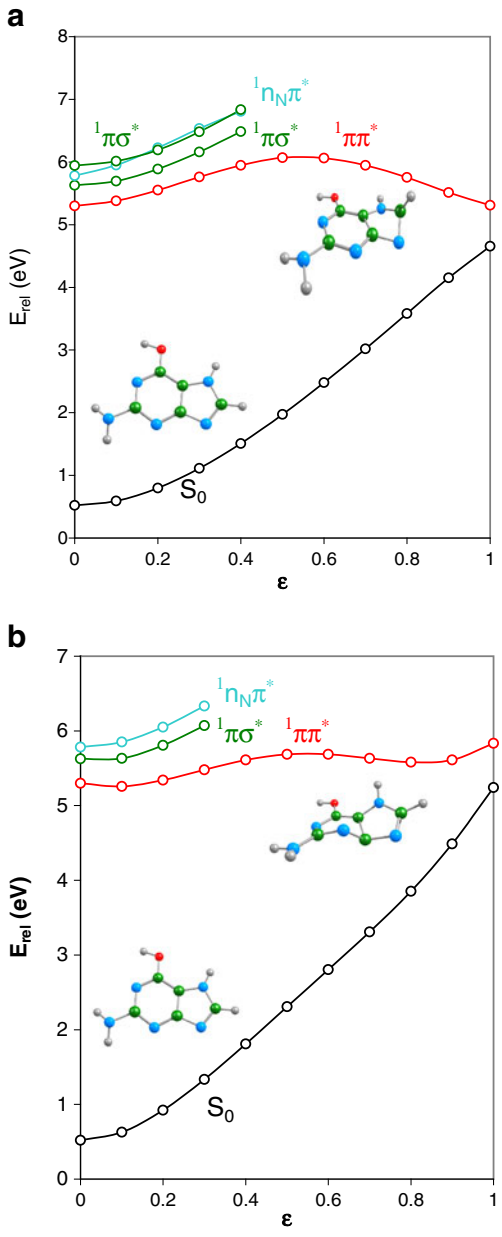

Fig. 5 Excited-state reaction paths of the transformations (**a**) A→CI_{A1} and (**b**) A→CI_{A2}. The CC2-energy of tautomer B (−541.209822 a.u.) is used as a reference value in calculating E_{rel}

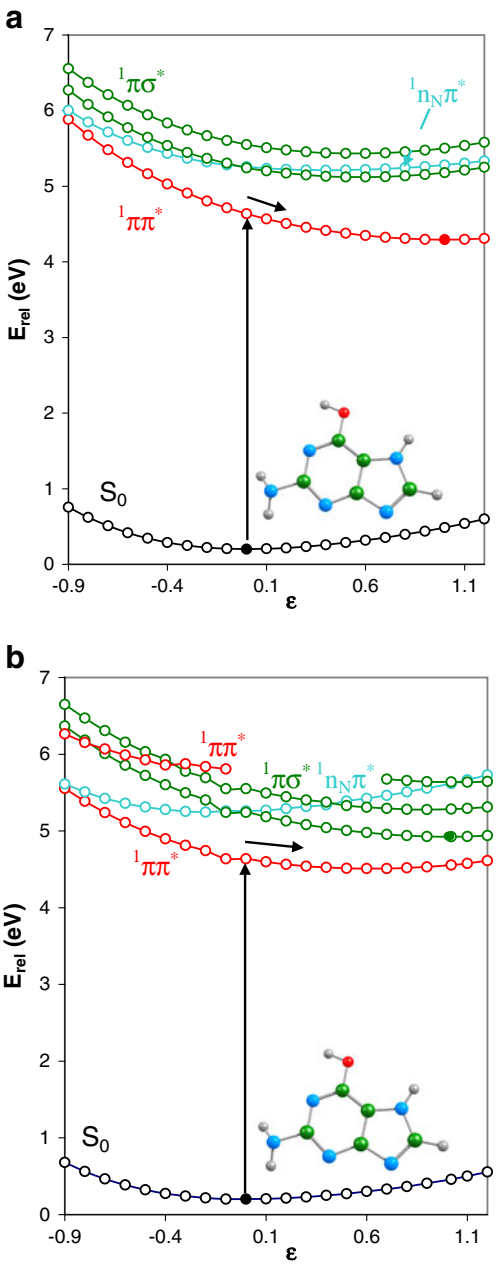

Fig. 6 Linearly interpolated reaction paths of the electronic states between (**a**) S_0 and S_1 ($^1\pi\pi^*$) and (**b**) S_0 and S_2 ($^1\pi\sigma^*$). *Solid circles* Position of the optimized equilibrium geometries. The reaction coordinates are extrapolated in two directions: $\varepsilon<0$ and $\varepsilon>1$. The CC2-energy of tautomer B (−541.209822 a.u.) is used as a reference value for the calculation of E_{rel}

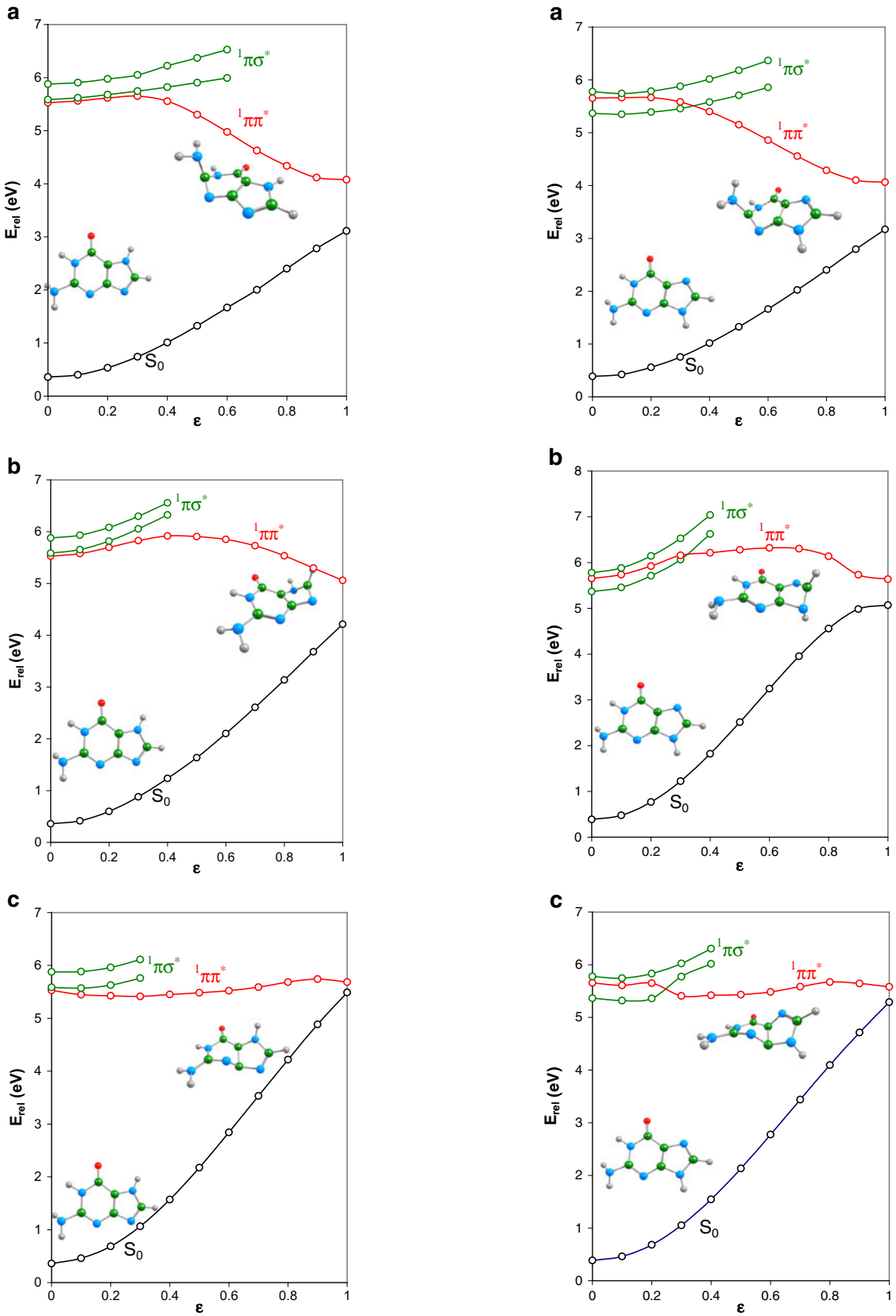

Fig. 7 Excited-state reaction paths for the transformations (**a**) B→CI_B, (**b**) B→CI_{B1}, and (**c**) B→CI_{B2}. The CC2-energy of tautomer B (−541.209822 a.u.) is used as a reference value for the calculation of E_{rel}

Fig. 8 Excited-state reaction paths of the transformations (**a**) C→CI_C, (**b**) C→CI_{C1}, and (**c**) C→CI_{C2}. The CC2-energy of tautomer B (−541.209822 a.u.) is used as a reference value for the calculation of E_{rel}

With the optimized equilibrium geometries of the S_0 and $^1\pi\pi^*$ excited states of tautomer A (CC2/aug-cc-pVDZ) we performed LIIC in order to check for the possibility of a population of higher-energy levels. The result is illustrated in Fig. 6a. The population of the $^1n_N\pi^*$ excited state occurs via conical intersection with high energy ($\varepsilon \approx -0.9$).

Figure 6b depicts the results from the LIIC between the equilibrium geometries of the S_0 and $^1\pi\sigma^*$ electronic states. The curves show again that the population of the $^1n_N\pi^*$ excited state occurs via conical intersection with high energy ($\varepsilon \approx -0.9$). As seen, the energy curve of the $^1n_N\pi^*$ excited state crosses the excited-state reaction paths of almost all excited states. In other words, the crossing points indicate the possibility of a switch between excited states.

The excited-state reaction paths of the ring deformation mechanisms of tautomer B are given in Fig. 7. As can be seen, the internal conversion of the $^1\pi\pi^*$ excited state through the conical intersection CI_B leads to the stabilization of the ground state of this tautomer. The energy curve does not show an energy barrier and implies a fs-relaxation of the excited state to the ground state. The $^1\pi\sigma^*$ excited-state reaction paths show an increase in energy along the reaction coordinates. For this approach, in the Franck-Condon region of the reaction coordinates, the energy of the lower-lying $^1\pi\sigma^*$ excited state is close to that of the $^1\pi\pi^*$ excited state.

The LIIC approach showed that the $^1\pi\pi^*$ excited-state reaction paths of the transformation B→CI_{B1} passes through a low energy barrier of 0.39 eV (38 kJ.mol^{-1}). Otherwise, this reaction path also shows that this guanine tautomer should be photostable with respect to the proposed $^1\pi\pi^*$ deactivation channel.

Figure 7c shows that the energy of the conical intersection CI_{B2} is almost equal to that of the $^1\pi\pi^*$ excited-state in the Franck-Condon area. The excited-state reaction path of this excited state leads to the conical intersection CI_{B2} and shows a very low energy barrier near the conical intersection. The mechanism implies a competitive fluorescent transition and an internal conversion through the conical intersection.

The excited-state reaction paths of the deformation mechanisms of tautomer C are illustrated in Fig. 8. They are very similar to those of tautomer B. The $^1\pi\sigma^*$ excited-state reaction path shows a difference: it crosses the $^1\pi\pi^*$ excited-state curve and in this way indicates the possible existence of a population of the $^1\pi\sigma^*$ excited state of tautomer C.

Similar results were obtained for tautomer B (Fig. 9). A crossing between the $^1\pi\sigma^*$ and $^1\pi\pi^*$ excited state was found only for the transformation D→CI_{D1}. In the remaining cases,

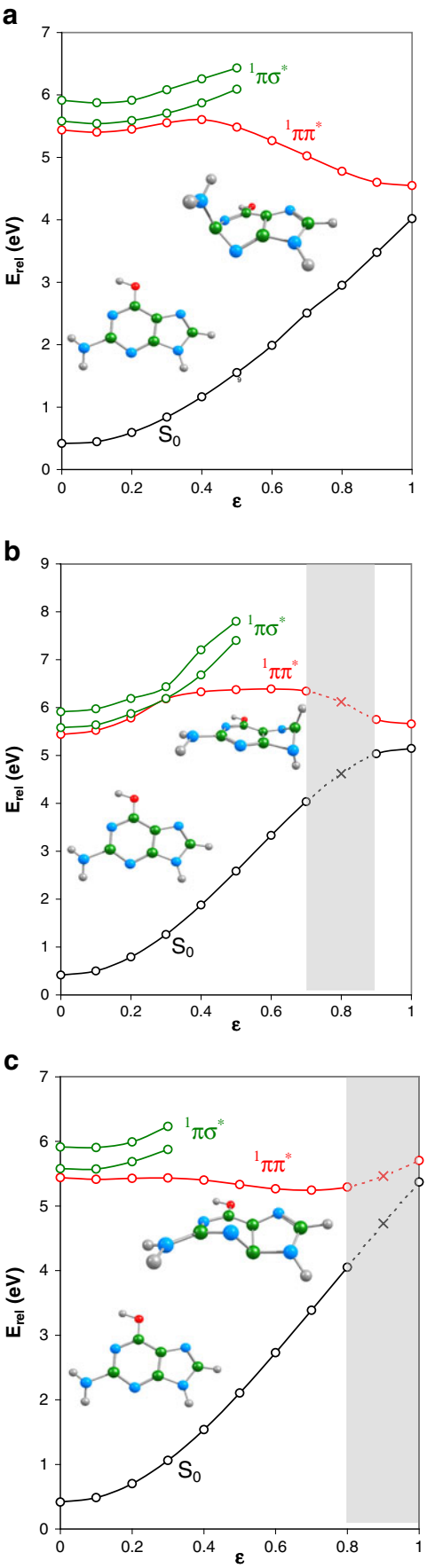

Fig. 9 Excited-state reaction paths of the transformations (**a**) D→CI_D, (**b**) D→CI_{D1}, and (**c**) D→CI_{D2}. The CC2-energy of tautomer B (−541.209822 a.u.) is used as a reference value for the calculation of E_{rel}. The *x-points* in the *gray field* were found by graphical interpolation

the $^1\pi\sigma^*$ excited state has higher energy than the $^1\pi\pi^*$ state. The transformation $D \rightarrow CI_{D2}$ is hindered by the high energy of the conical intersection CI_{D2}. In other words, this deformation either does not occur or occurs at a very low rate compared to the transformation $D \rightarrow CI_D$.

The observed energy gaps between the two electronic states at the conical intersections are expected because of switching from the CASSCF to the CC2 method. Perhaps the conical intersections at the CC2 level are left- or right-shifted along the concrete reaction coordinate. Unfortunately, the CC2 method cannot optimize the structures of the conical intersections.

Conclusions

This study of deformation mechanisms showed that the conical intersections S_0/S_1 are accessible through the $^1\pi\pi^*$ excited states of tautomers. The barrierless excited-state reaction paths for the deformations of tautomers at the amino group were determined. Obviously, these represent the ultrafast deactivation channels of guanine tautomers. Analysis of the linearly interpolated reaction paths showed that the tautomers of guanine should be photostable when exposed to UV light. The constructed adiabatic and quasi-diabatic PESs around each conical intersection revealed the nature of the conical intersections and showed that they are real mediators between the two electronic states, S_0 and S_1, responsible for internal conversion processes. The conical intersections of the processes of deformations at the pyrimidine ring have very high energies, commensurable with the excitation energies of the $^1\pi\pi^*$ excited states of tautomers. This means that these mechanisms are energetically disfavored. For tautomers C and D, crossings $^1\pi\pi^*/^1\pi\sigma^*$ were found. These are potential "switch-points" through which the $^1\pi\sigma^*$ excited states can be populated. Further, these states could participate in the photoinduced dissociation-association (PIDA) mechanism [21, 22] that explains the NH- and OH-dissociations in tautomers. These mechanisms will form the subject of further research.

Acknowledgment The author thanks the National Science Fund of Bulgaria, Project RNF01/0110 for technical support of the calculations (Linux-cluster MADARA).

References

1. Plekan O, Feyer V, Richter R, Coreno M, Vall-llosera G, Prince KC, Trofimov AB, Zaytseva IL, Moskovskaya TE, Gromov EV, Schirmer J (2009) J Phys Chem A 113:9376–9385
2. Choi MY, Miller RE (2006) J Am Chem Soc 128:7320–7328
3. Piuzzi F, Mons M, Dimicoli I, Tardivel B, Zhao Q (2001) Chem Phys 270:205–214
4. Plekan O, Feyer V, Richter R, Coreno M, de Simone M, Prince KC, Trofimov AB, Gromov EV, Zaytseva IL, Schirmer J (2008) Chem Phys 347:360–375
5. Mons M, Dimicoli I, Piuzzi F, Tardivel B, Elhanine M (2002) J Phys Chem A 106:5088–5094
6. Szczesniak M, Szczesniak K, Kwiatkowski JS, KuBulat K, Person WB (1988) J Am Chem Soc 110:8319–8330
7. Nir E, Plützer C, Kleinermanns K, de Vries M (2002) Eur Phys J D 20:317–329
8. Shukla MK, Leszczynski J (2006) Chem Phys Lett 429:261–265
9. Pugliesi I, Müller-Dethlefs K (2006) J Phys Chem A 110:13045–13057
10. Canuel C, Mons M, Piuzzi F, Tardivel B, Dimicoli L, Elhanine M (2005) J Chem Phys 122:074316(6)
11. Kistler KA, Matsika S (2008) J Chem Phys 128:215102(14)
12. Kistler KA, Matsika S (2007) J Phys Chem A 111:2650–2661
13. Matsika S, Krause P (2011) Annu Rev Phys Chem 62:621–643
14. Delchev VB, Sobolewski AL, Domcke W (2010) Phys Chem Chem Phys 12:5007–5015
15. Yamazaki S, Domcke W, Sobolewski A (2008) J Phys Chem A 112:11965–11968
16. Domcke W, Yarkony DR, Köppel H (2004) Conical intersections. World Scientific Press, Singapore
17. Woywod C, Domcke W, Sobolewski AL, Werner H-J (1994) J Chem Phys 100:1400–1413
18. Ahlrichs R, Baer M, Haeser M, Horn H, Koelmel C (1989) Chem Phys Lett 162:165–169
19. Hättig C, Weigend F (2000) J Chem Phys 113:5154–5161
20. Frisch MT et al (2004) Gaussian 03, Revision D.01. Gaussian, Wallingford
21. Sobolewski AL (1993) Chem Phys Lett 211:293–299
22. Chmura B, Rode M, Sobolewski AL, Lapinski L, Nowak M (2008) J Phys Chem A 112:13655–13661